Small Scale Anisotropy in Axisymmetric Turbulence

Douglas W. Carter

Department of Aerospace Engineering
University of Minnesota
110 Union St. SE 55455-0153
carte775@umn.edu

Alec J. Petersen

Department of Aerospace Engineering
University of Minnesota
110 Union St. SE 55455-0513
fcoletti@umn.edu

Filippo Coletti

Department of Aerospace Engineering
University of Minnesota
110 Union St. SE 55455-0513
fcoletti@umn.edu

ABSTRACT

We experimentally investigate the presence of anisotropy from the inertial to the dissipative scales in homogeneous turbulence. We employ an apparatus in which two facing arrays of randomly actuated air jets generate turbulence with negligible mean flow and shear, over a volume several times larger than the energy-containing eddy size. The Reynolds number based on the Taylor microscale is varied in the range $Re_\lambda \approx 300-500$, while the axial-to-radial ratio of the root mean square velocity fluctuations ranges between 1.37 and 1.72. Two velocity components are measured by particle image velocimetry (PIV) capturing from the inertial to the Kolmogorov scales and yielding statistics up to sixth order. The scaling exponents of the velocity structure functions are found to differ not only between the longitudinal and transverse components, but also between the axial and radial directions of separation. At the dissipative scales, the moments of the velocity gradients indicate that departure from isotropy is, at the present Reynolds numbers, significant and more pronounced for stronger large-scale anisotropy. The structure-function based measures of isotropy tend towards isotropy as the separation is reduced from the inertial to the near-dissipative scales (down to about 10η, η being the Kolmogorov length) but become more anisotropic for even smaller scales which are characterized by high intermittency.

I. INTRODUCTION

Ever since Kolmogorov (1941) (K41 for brevity) a common assumption in the study of turbulence is isotropic symmetry of small scales (at sufficient Reynolds number). The postulate of local isotropy and its implications have been scrutinized and debated for decades. Browne *et al.* (1987) and George & Hussein (1991) compiled some of the available results of laboratory studies up to $Re_\lambda = 990$, underscoring that the mean square derivatives of the velocity fluctuations were not consistent with local isotropy. Saddoughi & Veeravalli (1994), with their landmark measurements in the boundary layer of the NASA Ames wind tunnel at $Re_\lambda = 1450$, found significant support to local isotropy for statistics up to the second order. Ouellette *et al.* (2006) used a double impeller apparatus to measure Lagrangian structure functions at $Re_\lambda = 815$, finding that large-scale asymmetries were reflected already in the second-order statistics.

Local isotropy has been most often assumed in turbulence theories and models, but exceptions have become more frequent in the last decades. Durbin & Speziale (1991) argued on theoretical grounds that the small scales cannot be isotropic in the presence of a steady background strain, independently of the Reynolds number. Yeung & Brasseur (1991) performed low Re_λ simulations in triply periodic domains using asymmetric forcing, and showed that the small scales are affected by large scale anisotropy as a consequence of non-local triadic interactions in wavenumber space. As these interactions are thought to become stronger with scale separation, they speculated that small-scale anisotropy would exist also at asymptotically large Reynolds numbers. This idea found support in later simulations at much higher Reynolds numbers (Mininni *et al.*, 2006).

In the following we present results of an experimental study aimed to advance our understanding of turbulence anisotropy, from the inertial to the dissipative scales, providing complementary insights with respect to previous studies. To this end, PIV measurements are carried out in a recently introduced facility that generates homogeneous, shearless, anisotropic turbulence in the range $Re_\lambda = 298-496$. The facility and PIV measurements are discussed in §II., the results are presented in §III. and §IV., and conclusions and future work are discussed in §V..

II. APPARATUS AND METHODOLOGY
ZERO-MEAN FLOW TURBULENCE CHAMBER

The experimental apparatus and instrumentation was presented and qualified in Carter *et al.* (2016), and only a brief description will be given here. The facility consists of a 5 m^3 chamber in which full optical access is provided by the acrylic walls and ceiling. Two facing panels within the chamber accommodate arrays of 128 ports each, fed by pressurized air at 700 kPa and controlled by solenoid valves. The latter are individually actuated to fire quasi-synthetic air jets in randomized sequence, according to the algorithm proposed by Variano & Cowen (2008). The jet interaction produces turbulence which is approximately homogeneous, with no mean shear and negligible mean flow over a volume of $\approx$ 0.5 x 0.7 x 0.4 m^3 at the centre of the chamber. A conceptual sketch of the chamber is provided in figure 1; x_1 indicates the direction parallel to the jet axis, x_2 and x_3 are the transverse (vertical and horizontal, respectively) directions. Given the jet array configuration we assume axisymmetry about x_1 (for example when calculating dissipation, see §III). The Reynolds number can be adjusted by varying the average firing time of the jets (μ_{on}), as increasing the latter results in an increase of both the length scales and the rms velocity fluctuations. Here we consider five cases with μ_{on} ranging between 100 ms and

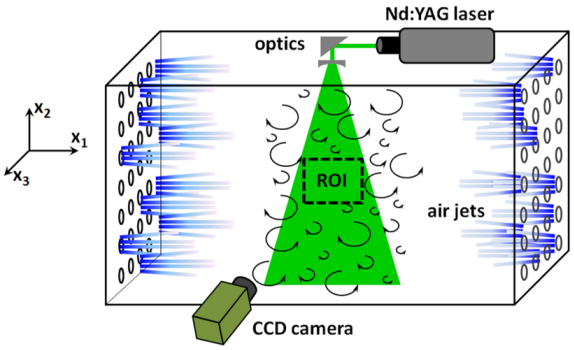

Figure 1. Illustration of the experimental setup.

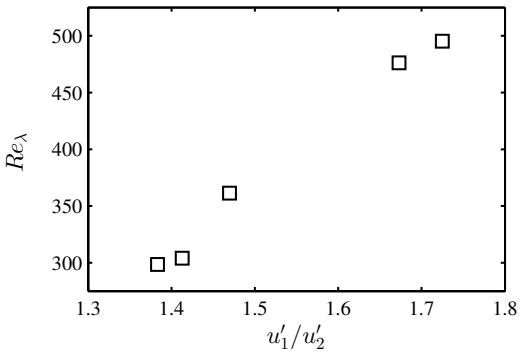

Figure 2. Reynolds number based on the Taylor microscale plotted versus anisotropy ratio.

3.2 s.

The facility is inspired by the jet-stirred water tank of Bellani & Variano (2014), which produces isotropic turbulence at the large scales. Here, on the other hand, significant large-scale anisotropy is present, and indeed the resulting turbulent flow possesses several features that make it especially well suited for investigating scale-to-scale anisotropy. Firstly, the homogeneity allows neglecting the effect of the spatial gradient of turbulent kinetic energy typical of decaying grid turbulence (Maxey, 1987). Secondly, the lack of mean shear allows investigating the anisotropy without the influence of complex shear production mechanisms (Veeravalli & Warhaft, 1989; Mydlarski & Warhaft, 1996; Biferale & Toschi, 2001). In the present system, as in other recently introduced devices featuring planar jet arrays (Khorsandi *et al.*, 2013; Bellani & Variano, 2014), the large homogeneous region allows for the natural development of the full energy cascade without the influence of mean shear or strain. Finally, the lack of mean flow is beneficial for the measurement accuracy.

VELOCITY MEASUREMENTS

PIV measurements are performed along the $x_1 - x_2$ symmetry plane at the center of the chamber. The flow is seeded with 1-2 μm DEHS (Di-Ethyl-Hexyl-Sebacate) droplets, illuminated by a 532 nm Nd:YAG laser, and imaged by a 4 megapixel CCD camera. The laser pulse separation is chosen such that the particle displacement is limited to 4-5 pixels to reduce out-of-plane loss of particles. Velocity fields are processed using an iterative cross-correlation algorithm, with final interrogation windows of 32 x 32 pixels and 50% overlap. Measurements are obtained by mounting a Nikon lense of 200 mm focal length. This provides a field of view (FOV) small enough to capture the dissipative scales of the flow (see table 1). Spatial derivatives are calculated with a second-order central difference scheme, after applying on the velocity fields a Gaussian filter with a kernel size matching the interrogation window size (Ganapathisubramani *et al.*, 2007).

Table 1. Basic imaging parameters for the PIV measurements.

Focal length [mm]	200
Field of View [cm x cm]	3.3 x 3.3
Vector Spacing [mm (η)]	0.31 (1-1.5)

For the considered cases, the relation between Re_λ and u_1'/u_2' are reported in figure 2. We calculate large-scale quantities (e.g. anisotropy ratio, integral scales) from a set of low-resolution/large-FOV measurements obtained for the same experimental settings, while the small-scale quantities (turbulent dissipation and related quantities) are based on high-resolution/small-FOV measurements. The anisotropy ratios between both resolutions are confirmed to agree within a few percent. For all cases the anisotropy ratio u_1'/u_2' is significantly larger than 1 (u_1, u_2, and u_3 are the fluctuating velocity components in direction x_1, x_2, and x_3, respectively, and the prime denotes rms quantities). In the considered range of jet array forcing parameters, increasing the average firing time of the jets leads to both higher Re_λ and larger u_1'/u_2'. This prevents us from independently assessing the influence of both parameters on the turbulence properties, but will not affect our main conclusions. Because the relation between Re_λ and u_1'/u_2' is roughly linear (figure 2) in the following the various quantities will be plotted as a function of Reynolds number, implying similar trends with large-scale anisotropy.

III. DISSIPATIVE RANGE ANISOTROPY

A common strategy to test the postulate of local isotropy at the dissipative scales is to evaluate moments of the velocity derivatives. In particular, following the ansatz of Taylor (1935), several authors have evaluated the ratios of the mean square velocity derivatives along different directions and compared them against the expected isotropic values (e.g. Browne *et al.*, 1987; George & Hussein, 1991; Tsinober *et al.*, 1992; Shafi & Antonia, 1997; Burattini *et al.*, 2010; Gomes-Fernandes *et al.*, 2012; Thiesset *et al.*, 2013; Valente & Vassilicos, 2014). Here we consider the following ratios, which should all be equal to one in isotropic turbulence:

$$K_1 = 2\langle a_{11}^2\rangle/\langle a_{21}^2\rangle \quad (1)$$

$$K_3 = 2\langle a_{11}^2\rangle/\langle a_{12}^2\rangle \quad (2)$$

$$K_5 = 2\langle a_{22}^2\rangle/\langle a_{12}^2\rangle \quad (3)$$

$$K_7 = 2\langle a_{22}^2\rangle/\langle a_{21}^2\rangle. \quad (4)$$

where $a_{ij} = \partial u_i/\partial x_j$. The nomenclature changes among different research groups; when possible we have followed the notation often used by Antonia and coworkers. The following quantities are also expected to be equal to one in K41:

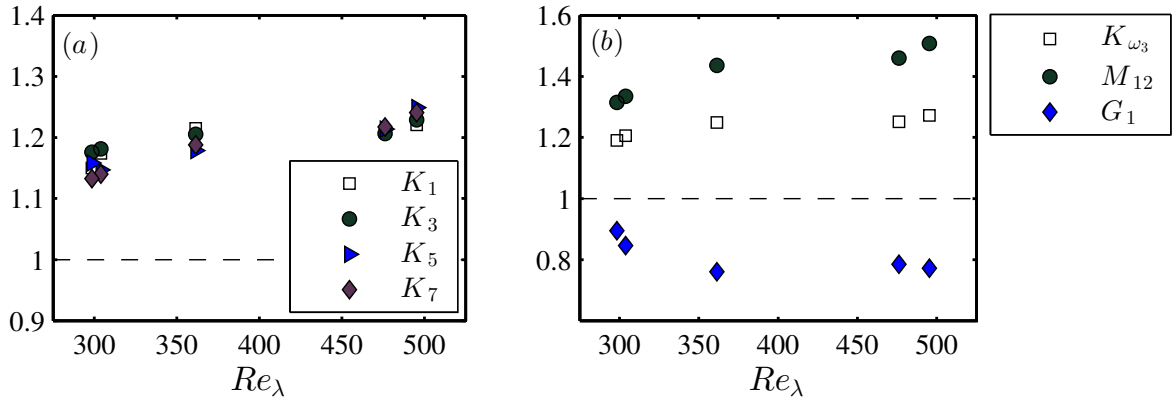

Figure 3. Small scale ratios for testing isotropy defined by equations (1) - (4) (a) and (5) - (7) (b). The dashed line in both panels indicates the isotropic value of 1.

$$K_{\omega_3} = \frac{5\langle a_{11}^2 \rangle}{\langle \omega_3^2 \rangle} \tag{5}$$

$$M_{12} = -\frac{1}{2}\frac{\langle a_{11}^2 \rangle}{\langle a_{12} a_{21} \rangle} \tag{6}$$

$$G_1 = \frac{3}{2}\frac{\langle a_{12} a_{21}^2 \rangle}{\langle a_{11}^3 \rangle} \tag{7}$$

where ω_3 is here the out-of-plane vorticity component. We remark that $M_{12} = 1$ only requires axisymmetry around the x_1 axis. While (1) to (6) are ratios of second-order moments, (7) is a third-order quantity and therefore $G_1 = 1$ may be expected to be a more stringent isotropy test. The values reported in literature for these ratios are fairly scattered, even for similar flow configurations. K_1 (the ratio reported most often) was found to be larger than one in most previous studies of free shear flows (e.g. Browne *et al.*, 1987; Hussein, 1994, among others), turbulent boundary layers (Shafi & Antonia, 1997), and grid turbulence (Tsinober *et al.*, 1992; Antonia *et al.*, 1998, among many others). K_3 was found to be smaller than one in various types of turbulent flows, although values larger than one were also reported in jets (Hussein, 1994) and grid turbulence (Gomes-Fernandes *et al.*, 2012). K_5 and K_7 were found to be larger than one in both wake flows (Browne *et al.*, 1987) and grid turbulence (Tsinober *et al.*, 1992), with K_7 typically larger than K_5. Some studies, e.g. Shafi & Antonia (1997), found K_{ω_3} in general agreement with isotropy, reflecting the fact that, in their measurements, $K_1 > 1$ and $K_3 < 1$.

The ratios (1) to (7) for the present flow are plotted as a function of Re_λ in figure 3. We remind that, in the present setup, increasing Re_λ implies increasing u_1'/u_2'. All K_i ratios are significantly larger than one. The level of small-scale anisotropy suggested by these values is significantly higher than what was found, e.g., by Lavoie *et al.* (2007) who had an essentially isotropic flow at the large scales. Among the K_i ratios, K_{ω_3} is furthest from isotropy, likely because here K_1 and K_3 are both larger than one. G_1 is significantly further from unity than the K_i ratios, which is expected being the former a third-order quantity. M_{12} on the other hand is also distant from isotropy, despite the fact that $M_{12} = 1$ only requires small-scale axisymmetry. All ratios depart from the isotropic value of one with increasing Re_λ, hence with increasing u_1'/u_2'. The increase in Reynolds number is expected to promote the return to isotropy at the small scales, but apparently the influence of large-scale anisotropy is strong enough to offset this tendency. This points to a direct link between anisotropy at the energetic and dissipative scales.

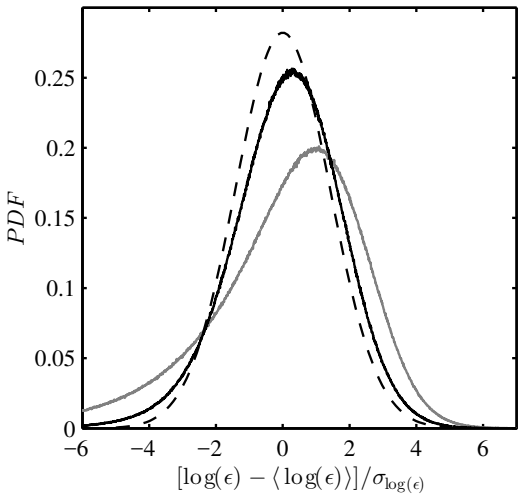

Figure 4. Normalized PDF of the logarithm of dissipation ε calculated under axisymmetric assumptions (black) and under isotropic assumptions (grey) for the case $Re_\lambda = 476$. A lognormal distribution is plotted for comparison (dashed.)

The fact that M_{12} is significantly larger than one suggests caution in assuming axisymmetry, at least at the smallest scales. We explore this issue by comparing the spatial distribution of local dissipation calculated both using local isotropy ($\varepsilon = 15\nu\langle a_{11}^2 \rangle$, as in the majority of studies relying on single-point velocity measurements) and using local axisymmetry (George & Hussein, 1991):

$$\varepsilon = \nu[-\langle a_{11}^2 \rangle + 2\langle a_{12}^2 \rangle + 2\langle a_{21}^2 \rangle + 8\langle a_{22}^2 \rangle]. \tag{8}$$

The refined similarity hypotheis (Kolmogorov, 1962) postulates a log-normal distribution of ε to account for the internal intermittency of turbulence. Although some authors have pointed out theoretical inconsistencies in this assumption (see Frisch, 1995), evidence from the bulk of experimental and numerical studies in the literature seems to support it (e.g. Wang *et al.*, 1996; Chen *et al.*, 1997; Mullin & Dahm, 2006; Ganapathisubramani *et al.*, 2008). Figure 4 indicates that, while the dissipation calculated using axisymmetry shows significant departure from log-normality for the low ε values, it does approximate such behavior much more closely

compared to the isotropic assumption.

IV. INERTIAL RANGE ANISOTROPY

To address the propagation of anisotropy through the inertial scales we investigate the structure functions defined over separation $\boldsymbol{r}$:

$$D_{ii}^n(\boldsymbol{r}) = \langle [u_i(\boldsymbol{x}+\boldsymbol{r}) - u_i(\boldsymbol{x})]^n \rangle \tag{9}$$

which in homogeneous flows is independent of the position vector $\mathbf{x}$. According to K41, for separations r_j in the inertial range:

$$D_{ii}^n(r_j) = C_n(\varepsilon r_j)^{\zeta_n}. \tag{10}$$

K41 further predicts $\zeta_n = n/3$ and C_n being constant. We distinguish between the longitudinal structure functions (LSF), for which the velocity component u_i is parallel to the separation, and the transverse structure function (TSF), for which u_i is normal to it. In the following we denote them as D_L^n and D_T^n, respectively. The inertial range is classically identified as the separation interval over which the third-order LSF scales linearly with r_j (from $\zeta_3 = 1$). LSFs and TSFs, and especially their scaling properties, have been explored in many studies investigating scale-to-scale turbulence dynamics. Unlike in most previous experiments using point-wise techniques, PIV provides access to both LSF and TSF associated to displacements along two directions: the axial direction x_1 and the radial direction x_2. Therefore, we are able to investigate the four quantities $D_L^n(r_1) = D_{11}^n(r_1)$, $D_L^n(r_2) = D_{22}^n(r_2)$, $D_T^n(r_2) = D_{11}^n(r_2)$, and $D_T^n(r_1) = D_{22}^n(r_1)$ which according to the postulate of local isotropy should all have the same scaling behavior. This is explicitly tested for in the following, along with other isotropic relations.

SCALING EXPONENTS OF N-TH ORDER STUCTURE FUNCTIONS

We consider the scaling exponents of the nth-order structure functions. These have been investigated in depth in the past, especially as they relate to intermittency and the consequent anomalous scaling, i.e. the departure from the K41 prediction $\zeta_n = n/3$ (Anselmet *et al.*, 1984; Siebert & Warhaft, 2010, among many others). The scaling exponents have been studied extensively also in the context of local isotropy, comparing the behavior of velocity differences in different directions, but without reaching consensus on their trend.

Here we calculate LSF and TSF up to the sixth order, with separations along both axial (i.e. $\zeta_n^{L,1}$, $\zeta_n^{T,1}$) and radial ($\zeta_n^{L,2}$, $\zeta_n^{T,2}$) directions. Premultiplied probability density functions for velocity separations from the smallest to the inertial scales were used to confirm statistical convergence up to sixth order. We obtain the scaling exponents following the extended self-similarity (ESS) approach proposed by Benzi *et al.* (1993). In ESS, the structure function of interest is plotted against a structure function of different order, rather than against the physical separation. This significantly extends the scaling range, partly because the sampling undulations are generally correlated among structure functions of different orders (Frisch, 1995). The procedure is particularly straightforward when plotting against the third-order LSF, which works as a surrogate for the separation if one assumes $\zeta_3^L = 1$. Moreover, to improve statistical convergence of the odd order moments, it is customary to consider structure functions of the absolute value of the velocity difference, $D_{ii}^{|n|}(r) = \langle |u_i(x+r) - u_i(x)|^n \rangle$, which have marginally different scaling with respect to D_{ii}^n (Benzi *et al.*, 1993; Sreenivasan *et al.*, 1996).

The ESS-based scaling exponents for LSF and TSF (in both axial and radial directions) for cases $Re_\lambda = 298$ and 476 are reported in table 2. These are calculated over the range for which the logarithmic relative slope of the third-order LSF to the absolute-valued third-order LSF is equal to one within ∼4%. This corresponds to separations in the approximate range 15η - 40η and varies slightly depending on the case. The dominant uncertainties in the exponents stem from the standard error of the slopes in the straight line fits and the chosen bound on the ESS scaling range, as these are typically much larger than the error due to measurement or statistical uncertainty. In figure 5 the exponents are compared with the K41 scaling $\zeta_n = n/3$ and with the model of She & Leveque (1994). The latter is an intermittency model that assumes a hierarchical distribution of the energy dissipation rate and predicts:

$$\zeta_n = \frac{n}{9} + 2[1 - (\frac{2}{3})^{n/3}]. \tag{11}$$

The LSF scaling exponent measured with separation in the axial direction, which is the most commonly reported in literature, appears remarkably close to the She & Leveque (1994) model, especially at the higher Reynolds numbers. In figure 5 the case at $Re = 476$ is also compared with the benchmark experiments of Shen & Warhaft (2002) (unsheared grid turbulence at $Re_\lambda = 863$ and $u_1'/u_2' = 1.71$). The agreement in terms of $\zeta_n^{L,1}$ is excellent, seemingly supporting the statement of Ishihara *et al.* (2009) that LSFs show a universal behavior independent on the large-scale flow conditions.

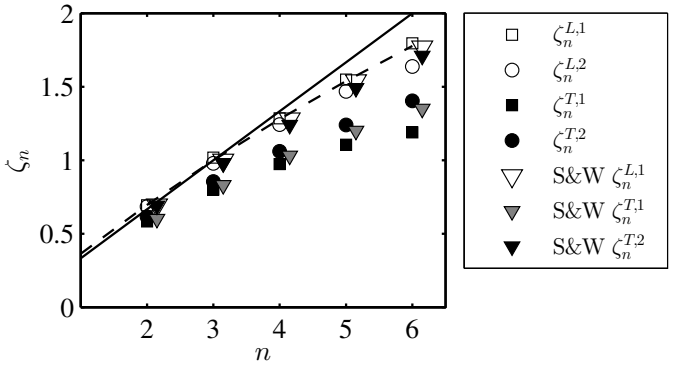

Figure 5. K41 model (black line) and the model of She & Leveque (1994) (dashed), $\zeta_n^{L,1}$, $\zeta_n^{L,2}$, $\zeta_n^{T,1}$, and $\zeta_n^{T,2}$ for the case $Re_\lambda = 476$. Comparison with the data of Shen & Warhaft (2002) offset to the right along the abscissa for clarity.

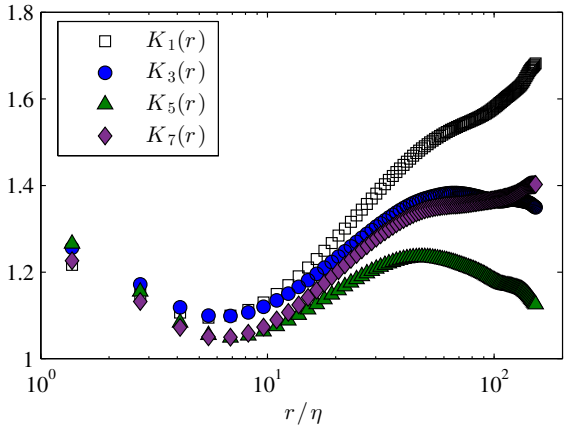

Figure 6. Structure function based measures of isotropy $K_i(r)$ for the case $Re_\lambda = 298$.

Table 2. Scaling exponents of structure functions for two representative cases obtained using ESS (Benzi *et al.*, 1993) with estimated uncertainties in brackets.

	$Re_\lambda = 298$, $u_1'/u_2' = 1.38$					$Re_\lambda = 476$, $u_1'/u_2' = 1.72$				
	$n=2$	$n=3$	$n=4$	$n=5$	$n=6$	$n=2$	$n=3$	$n=4$	$n=5$	$n=6$
$\zeta_n^{L,1}$	0.69 [0.04]	0.98 [0.06]	1.28 [0.07]	1.53 [0.08]	1.77 [0.11]	0.70 [0.04]	1.00 [0.07]	1.28 [0.07]	1.54 [0.12]	1.77 [0.25]
$\zeta_n^{L,2}$	0.67 [0.04]	0.96 [0.05]	1.22 [0.07]	1.44 [0.09]	1.63 [0.10]	0.69 [0.04]	0.98 [0.05]	1.25 [0.07]	1.47 [0.08]	1.64 [0.08]
$\zeta_n^{T,1}$	0.57 [0.03]	0.79 [0.04]	0.97 [0.05]	1.11 [0.07]	1.22 [0.09]	0.59 [0.04]	0.81 [0.06]	0.98 [0.07]	1.11 [0.08]	1.19 [0.09]
$\zeta_n^{T,2}$	0.60 [0.03]	0.84 [0.04]	1.04 [0.06]	1.21 [0.07]	1.37 [0.08]	0.61 [0.03]	0.84 [0.05]	1.04 [0.07]	1.20 [0.07]	1.34 [0.09]

Figure 5 also confirms that the TSF exponents are significantly smaller than the LSF exponents, as consistently reported in the literature (Romano & Antonia, 2001; Ishihara *et al.*, 2009, and references therein). Our values of $\zeta_n^{T,1}$ are in fair agreement with those of Shen & Warhaft (2002) and Zhou *et al.* (2001), whereas in the DNS of Gotoh *et al.* (2002) the difference between the LSF and TSF scaling exponents is much smaller. This indicates that significant large-scale anisotropy (absent in the DNS) crucially contributes to the inequality $\zeta_n^T < \zeta_n^L$.

STRUCTURE FUNCTION BASED ISOTROPY MEASURES

In order to investigate the scale-to-scale isotropy, we utilize the same measures of isotropy in equations (1)-(4) using the appropriate structure functions, e.g.

$$K_1(\boldsymbol{r}) = \frac{2D_L^2(r_1)}{D_T^2(r_1)} \tag{12}$$

where $K_3(\boldsymbol{r})$, $K_5(\boldsymbol{r})$ and $K_7(\boldsymbol{r})$ are calculated analogously. The structure function based measures of isotropy are plotted in figure 6. The shape of the $K_i(r)$ functions appear to support the return to isotropy from $r/\eta \sim 150$ down to $O(10\eta)$, beyond which all measures show a departure from isotropy down to vanishing separation distance. This is believed to be a manifestation of dissipative-range intermittency (as opposed to inertial-range intermittency) as was discussed in detail by Chevillard *et al.* (2005). Dissipation-range intermittency has received much attention following the seminal observation of Kraichnan (1967) that any local variation of the dissipation rate produces the strongest fluctuations at the highest wavenumbers of the turbulence spectrum. It is noted that for increasing anisotropy ratio (and therefore also increasing Re_λ) the departure from isotropy is more pronounced (as was noted in §III.) This points to the influence of greater large scale anisotropy outweighing the influence of greater separation of scales.

V. CONCLUSIONS

Taken together, these results highlight the importance of considering, for a full characterization of all scales of the turbulence, not only the different velocity components but also the different spatial directions. A limitation of the present work is represented by the fact that the Reynolds number and the large-scale anisotropy cannot be varied independently in our apparatus, preventing firm conclusions on the respective quantitative influences of both parameters. Experimental facilities capable of disentangling the two effects, such as the turbulence chamber of Chang *et al.* (2012), are invaluable in this sense. We also remark the importance, in order to explore truly homogeneous turbulence, of generating a homogeneous region much larger than the integral scale. This has been achieved in the present set up at the cost of building a chamber of considerable size.

As it has been noted by several authors, anisotropy is deeply interrelated to intermittency at all scales (see, for e.g. Warhaft, 2009). The details of this relation, however, remain relatively unexplored. The present results suggest that intermittency models able to account for anisotropy, even implicitly, may stand a better chance of reproducing the observations. For example, the physical picture associated to the model of She & Leveque (1994) features small filamentary structures which are responsible for intermittency and dissipate energy at a rate constructed from a small-scale time and a large-scale velocity. Such a mixed scaling naturally opens up to incorporating large-scale anisotropy. In the present work we have not directly addressed the topology of the turbulent structures, nor the energy transfer among scales - aspects which are connected to the emergence of intermittency and the propagation of anisotropy, and which will be explored in a future study.

REFERENCES

Anselmet, F., Gagne, Y., Hopfinger, E. J. & Antonia, R. A. 1984 High-order velocity structure functions in turbulent shear flows. *Journal of Fluid Mechanics* **140** (-1), 63.

Antonia, RA, Zhou, T & Zhu, Y 1998 Three-component vorticity measurements in a turbulent grid flow. *Journal of Fluid Mechanics* **374**, 29–57.

Bellani, Gabriele & Variano, Evan A. 2014 Homogeneity and isotropy in a laboratory turbulent flow. *Experiments in Fluids* **55** (1), 1646.

Benzi, R., Ciliberto, S., Tripiccione, R., Baudet, C., Massaioli, F. & Succi, S. 1993 Extended self-similarity in turbulent flows. *Physical Review E* **48** (1), R29–R32.

Biferale, Luca & Toschi, Federico 2001 Anisotropic Homogeneous Turbulence: Hierarchy and Intermittency of Scaling Exponents in the Anisotropic Sectors. *Physical Review Letters* **86** (21), 4831–4834.

Browne, L W B, Antonia, R. a. & Shah, D. a. 1987 Turbulent energy dissipation in a wake. *Journal of Fluid Mechanics* **179** (-1), 307.

Burattini, P, Falchi, M, Romano, G P & Antonia, R A 2010 PIV and

hot wire measurements in the far field of turbulent round jets. *Measurement Science and Technology* **21** (12), 125402.

Carter, Douglas, Petersen, Alec, Amili, Omid & Coletti, Filippo 2016 Generating and controlling homogeneous air turbulence using random jet arrays. *Experiments in Fluids* **57** (12), 189.

Chang, Kelken, Bewley, Gregory P & Bodenschatz, Eberhard 2012 Experimental study of the influence of anisotropy on the inertial scales of turbulence. *J. Fluid Mech* **692**, 464–481.

Chen, Shiyi, Sreenivasan, Katepalli R., Nelkin, Mark & Cao, Nianzheng 1997 A Refined Similarity Hypothesis for Transverse Structure Functions. *Physical Review Letters* **79** (12), 4.

Chevillard, L., Mazellier, N., Poulain, C., Gagne, Y. & Baudet, C. 2005 Statistics of Fourier Modes of Velocity and Vorticity in Turbulent Flows: Intermittency and Long-Range Correlations. *Physical Review Letters* **95** (20), 200203.

Durbin, P. A. & Speziale, C. G. 1991 Local Anisotropy in Strained Turbulence at High Reynolds Numbers. *Journal of Fluids Engineering* **113** (4), 707.

Frisch, Uriel 1995 Turbulence (cambridge.

Ganapathisubramani, B., Lakshminarasimhan, K. & Clemens, N. T. 2007 Determination of complete velocity gradient tensor by using cinematographic stereoscopic PIV in a turbulent jet. *Experiments in Fluids* **42** (6), 923–939.

Ganapathisubramani, B., Lakshminarasimhan, K. & Clemens, N. T. 2008 Investigation of three-dimensional structure of fine scales in a turbulent jet by using cinematographic stereoscopic particle image velocimetry. *Journal of Fluid Mechanics* **598**, 141–175.

George, William K. & Hussein, Hussein J. 1991 Locally axisymmetric turbulence. *Journal of Fluid Mechanics* **233** (1991), 1.

Gomes-Fernandes, R, Ganapathisubramani, B & Vassilicos, J C 2012 Particle image velocimetry study of fractral-generated turbulence. *Journal of Fluid Mechanics* **711**, 306–336.

Gotoh, Toshiyuki, Fukayama, Daigen & Nakano, Tohru 2002 Velocity field statistics in homogeneous steady turbulence obtained using a high-resolution direct numerical simulation. *Physics of Fluids* **14** (3), 1065–1081.

Hussein, Hussein J. 1994 Evidence of local axisymmetry in the small scales of a turbulent planar jet. *Physics of Fluids* **6** (6), 2058.

Ishihara, Takashi, Gotoh, Toshiyuki & Kaneda, Yukio 2009 Study of HighReynolds Number Isotropic Turbulence by Direct Numerical Simulation. *Annual Review of Fluid Mechanics* **41** (1), 165–180.

Khorsandi, B, Gaskin, S & Mydlarski, L 2013 Effect of background turbulence on an axisymmetric turbulent jet. *J. Fluid Mech* **736**, 250–286.

Kolmogorov, Andrei N 1941 The local structure of turbulence in incompressible viscous fluid for very large reynolds numbers. In *Dokl. Akad. Nauk SSSR*, , vol. 30, pp. 301–305. JSTOR.

Kolmogorov, Andrey Nikolaevich 1962 A refinement of previous hypotheses concerning the local structure of turbulence in a viscous incompressible fluid at high reynolds number. *Journal of Fluid Mechanics* **13** (01), 82–85.

Kraichnan, Robert H. 1967 Inertial Ranges in TwoDimensional Turbulence. *Physics of Fluids (1958-1988)* **10** (7), 1417–1423.

Lavoie, P, Djenidi, L & Antonia, RA 2007 Effects of initial conditions in decaying turbulence generated by passive grids. *Journal of Fluid Mechanics* **585**, 395–420.

Maxey, MR 1987 The velocity skewness measured in grid turbulence. *The Physics of fluids* **30** (4), 935–938.

Mininni, P. D., Alexakis, A. & Pouquet, A. 2006 Large-scale flow effects, energy transfer, and self-similarity on turbulence. *Physical Review E* **74** (1), 016303.

Mullin, John A. & Dahm, Werner J. A. 2006 Dual-plane stereo particle image velocimetry measurements of velocity gradient tensor fields in turbulent shear flow. II. Experimental results. *Physics of Fluids* **18** (3), 035102.

Mydlarski, L. & Warhaft, Z. 1996 On the onset of high-Reynolds-number grid-generated wind tunnel turbulence. *Journal of Fluid Mechanics* **320** (-1), 331.

Ouellette, Nicholas T, Xu, Haitao, Bourgoin, Mickaël & Bodenschatz, Eberhard 2006 Small-scale anisotropy in Lagrangian turbulence. *New Journal of Physics* **8** (6), 102–102.

Romano, Giovanni Paolo & Antonia, Robert A 2001 Longitudinal and transverse structure functions in a turbulent round jet: effect of initial conditions and Reynolds number. *Journal of Fluid Mechanics* **436**, 231–248.

Saddoughi, Seyed G & Veeravalli, Srinivas V 1994 Local isotropy in turbulent boundary layers at high reynolds number. *Journal of Fluid Mechanics* **268**, 333–372.

Shafi, H. S. & Antonia, R. a. 1997 Small-scale characteristics of a turbulent boundary layer over a rough wall. *Journal of Fluid Mechanics* **342**, 263–293.

She, Zhen-Su & Leveque, Emmanuel 1994 Universal scaling laws in fully developed turbulence. *Physical Review Letters* **72** (3), 336–339.

Shen, X. & Warhaft, Z. 2002 Longitudinal and transverse structure functions in sheared and unsheared wind-tunnel turbulence. *Physics of Fluids* **14** (1), 370–381.

Siebert, H., Shaw R. A. & Warhaft, Z. 2010 Statistics of Small-Scale Velocity Fluctuations and Internal Intermittency in Marine Stratocumulus Clouds. *Journal of the Atmospheric Sciences* **67** (1), 262–273.

Sreenivasan, K. R., Vainshtein, S. I., Bhiladvala, R., San Gil, I., Chen, S. & Cao, N. 1996 Asymmetry of Velocity Increments in Fully Developed Turbulence and the Scaling of Low-Order Moments. *Physical Review Letters* **77** (8), 1488–1491.

Taylor, Geoffrey Ingram 1935 Statistical theory of turbulence. In *Proceedings of the Royal Society of London A: Mathematical, Physical and Engineering Sciences*, , vol. 151, pp. 421–444. The Royal Society.

Thiesset, F., Danaila, L. & Antonia, R. A. 2013 Dynamical effect of the total strain induced by the coherent motion on local isotropy in a wake. *Journal of Fluid Mechanics* **720**, 393–423.

Tsinober, A, Kit, E & Dracos, T 1992 Experimental investigation of the field of velocity gradients in turbulent flows. *Journal of Fluid Mechanics* **242** (-1), 169.

Valente, PC & Vassilicos, JC 2014 The non-equilibrium region of grid-generated decaying turbulence. *Journal of Fluid Mechanics* **744**, 5–37.

Variano, Evan A. & Cowen, Edwin A. 2008 full-text. *Journal of Fluid Mechanics* **604**, 1–64.

Veeravalli, S. & Warhaft, Z. 1989 The shearless turbulence mixing layer. *Journal of Fluid Mechanics* **207** (-1), 191.

Wang, Lian-Ping, Chen, Shiyi, Brasseur, James G & Wyngaard, John C 1996 Examination of hypotheses in the kolmogorov refined turbulence theory through high-resolution simulations. part 1. velocity field. *Journal of Fluid Mechanics* **309**, 113–156.

Warhaft, Zellman 2009 Why we need experiments at high reynolds numbers. *Fluid dynamics research* **41** (2), 021401.

Yeung, P. K. & Brasseur, James G. 1991 The response of isotropic turbulence to isotropic and anisotropic forcing at the large scales. *Physics of Fluids A: Fluid Dynamics* **3** (5), 884–897.

Zhou, T, Pearson, BR & Antonia, RA 2001 Comparison between temporal and spatial transverse velocity increments in a turbulent plane jet. *Fluid Dynamics Research* **28** (2), 127–138.